

A Kinematic Error Model for a Parallel Gantry-Tau Manipulator

Isolde Dressler, Torgny Brogårdh and Anders Robertsson

Abstract—Parallel robots are generally said to be more accurate but to have a smaller workspace compared to serial robots. With the Gantry-Tau robot, a parallel robot with a large, reconfigurable workspace was presented. This article tries to identify the maximum achievable end-effector positioning accuracy of the Gantry-Tau robot. To this end, a couple of new kinematic error models are presented and evaluated. The sources of the remaining positioning errors (0.09 mm) are discussed.

I. INTRODUCTION

Although today's industry still mostly uses serial robots, parallel kinematic robots have many advantages over serial robots. They are in general more accurate, stiffer and can reach higher accelerations [1]. Their inconvenience is however that their workspace is in general considerably smaller than that of a serial robot.

With the Gantry-Tau robot (Fig. 1) [2], a parallel kinematic manipulator (PKM) was presented that overcomes the inconvenience of a small workspace. Based on an ABB patent [3], it is a gantry version of the 3 degree-of-freedom (DOF) Tau PKM [4]. A slightly different Gantry-Tau variant is presented in [5], which has, unlike [2], a variable end-effector orientation. The possibility of a modular construction makes it convenient for flexible manufacturing processes (e.g. in small and medium sized enterprises) and the capability of prolonging the workspace to any customarized length is ideal for manufacturing of large size objects.

In [6], the authors presented kinematic calibration results of a small size Gantry-Tau prototype. The mean absolute positioning error of the tool center point (TCP) after calibration was shown to be around 200 μm . Recent measurements on the full size prototype show that the robot's repeatability is considerably better. In [7], the omni-directional repeatability of the TCP was shown to be 13 μm in the mean with a maximum of 50 μm .

To benefit to a larger extent from the Gantry-Tau robot's high repeatability, a more accurate kinematic model for positioning control is necessary. [4] and [5] introduced kinematic error models for the Tau robot and the Gantry-Tau robot with variable end-effector orientation. The kinematic error models cope with small manufacturing errors which are not part of



Fig. 1. Full size Gantry-Tau prototype (SMERobotTMproject)

the nominal model. [5] only examines errors in the actuator positioning and validates the approach by simulation.

Kinematic error models for numerous parallel manipulator architectures were presented in the past. An early example is [8], which presents a kinematic error model for a Stewart platform. To our knowledge the models presented were mostly verified by simulations and few results on the kinematic accuracy in practice exist.

In this article, we present a new kinematic error model for the Gantry-Tau robot and try to identify the maximum achievable end-effector positioning accuracy in practice. The validity of the nominal model assumptions on the actuators and arm structure are examined. Based on the results, a kinematic error model is proposed and evaluated by kinematic calibration using laser tracker measurements. A parameter sensitivity analysis is performed.

The article is organized as follows: In Sect. II, the Gantry-Tau robot is presented. Sect. III presents the kinematic error models adopted. Sect. V contains a discussion about the modeling and the calibration results presented in Sect. IV. Sect. VI concludes the article.

II. THE GANTRY-TAU ROBOT

The 3 DOF Gantry-Tau parallel robot (Figs 1, 2) consists of three kinematic chains. Each chain is driven by a linear actuator implemented as a cart moving on a linear guideway. The 3 carts are connected to the end-effector plate via link clusters consisting of a different number of links. The link clusters together with the end-effector plate are referred to as arm system in the following. The altogether 6 links are grouped in a 3-2-1 configuration and connected to the carts and the end-effector plate by spherical joints. Their placement on plate and carts according to the so-called Tau configuration is such that the links belonging to one cluster form parallelograms, which assures a constant end-

Isolde Dressler and Anders Robertsson are with the Department of Automatic Control, LTH, Lund University, SE-22100 Lund, Sweden, isolde.dressler@control.lth.se.

Torgny Brogårdh is with ABB Robotics, SE-72168 Västerås, Sweden.

This work has been funded by the European Commission's Sixth Framework Programme under grant no. 011838 as part of the Integrated Project SMERobotTM[10]. The authors would like to thank Casting Technology International, Boeing, Leica Geosystems and Güdel AG for supporting the measurements.

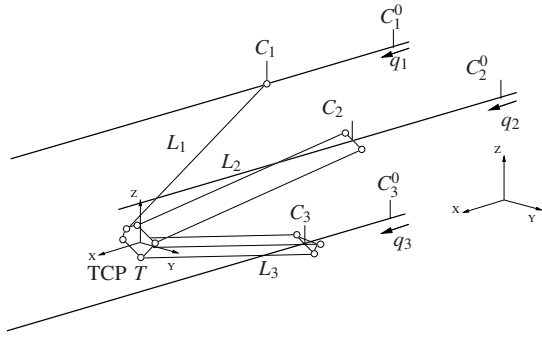


Fig. 2. Gantry-Tau schema with notation for variables and parameters

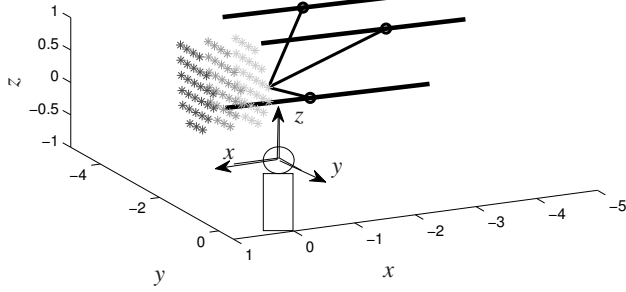


Fig. 3. Schema of simplified Gantry-Tau with points of TCP measurement set 1 (see Sect. III-B) and corresponding laser tracker positioning. Here, only every second measurement point layer is shown for better visibility (first layer to the left in the figure).

effector orientation. The Gantry-Tau robot has thus three purely translational DOFs.

III. KINEMATIC MODELING

A. Nominal Kinematics

A detailed solution of the kinematics problem can be found in [2] or [6]. Provided that the end-effector orientation is constant due to a perfect spherical joint placement, it is sufficient to consider the simplified robot shown in Fig. 3.

The closure equation for link i is then (notation see Fig. 2):

$$L_i^2 - \|T - {}^sC_i\|_2^2 = 0 \quad (1)$$

The cart position sC_i of the simplified model can be expressed as:

$${}^sC_i = {}^sC_i^0 + q_i \cdot v_i \quad (2)$$

where v_i is the unit vector in positive track i direction.

The track offset ${}^sC_i^0$ of the simplified model is

$${}^sC_i^0 = C_i^0 - R_T \cdot P_i \quad (3)$$

where P_i is link i 's spherical joint position on the end-effector plate expressed in TCP coordinates and R_T the rotation matrix between the TCP and the global frame.

The nominal kinematic model assumes perfectly linear actuators and constant end-effector orientation guaranteed by the Tau-configuration of the spherical joints.

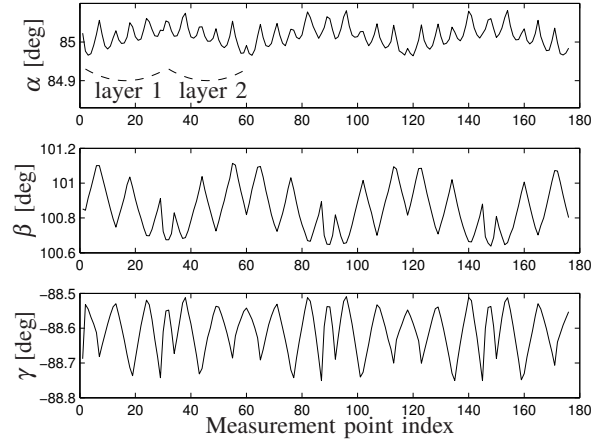


Fig. 4. Orientational error: ZYZ Euler angles of end-effector plate orientation measured along a grid (Fig. 3). The pattern corresponding to the grid point layers is marked out for layers 1 and 2, see upper figure.

B. Measurements

For kinematic calibration and evaluation of the model assumptions, the following measurement sets were recorded using a laser tracker with a Leica T-Mac and a corner cube reflector [9].

- 1) For each of 176 TCP poses lying on a grid filling the robot's workspace, the position and orientation of the 3 DOF end-effector were recorded with the T-Mac.
- 2) Independently from the above measurements, and with a different laser tracker positioning and thus expressed in a different coordinate frame, the cart position and orientation were measured for 28 points along the guideways with the T-Mac for each of the three carts. During these measurements, all carts were moved equally, so that the configuration of the arm system (the angles between the link clusters) and consequently the load on the carts did not change throughout the measurement. The TCP was located in the center of the workspace in $Y-Z$ direction.
- 3) In addition to the above actuator measurements, and with a third laser tracker positioning, the cart positions were recorded with a corner cube reflector while the TCP was moving to a set of 150 random poses.

C. Evaluation of Model Assumptions

In the following section, the assumptions of the nominal kinematics will be evaluated using the above measurements.

Fig. 4 shows the end-effector orientation represented as ZYZ Euler angles along the grid of measurement set 1. The maximal Euler angle variations lie between 0.1° (α) and 0.5° (β). The repeating pattern exhibited can be associated with the 6 grid layers orthogonal to the actuator axes that the TCP is traversing (the robot is moving forward in one layer and the same path backwards in the next layer, Fig. 3).

The pattern in Fig. 4 indicates that the TCP orientation errors are mainly caused by the arm system. Orientation variations of the carts along the guideways would have given

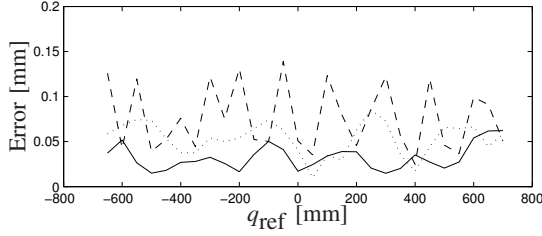


Fig. 5. Linearity error of actuators: Absolute value of residuals when fitting a linear function to the movement of cart 1 (solid), cart 2 (dashed) and cart 3 (dotted). Along the abscissa, the commanded cart position is shown.

variations between the layers for measurement points with the same Y - Z values (compare Fig. 3).

To examine the actuator linearity and positioning accuracy, measurement set 2 was evaluated. Fig. 5 shows the absolute value of the residuals when fitting a linear function according to Eq. (2) between commanded cart positions $q_i(k)$ and measurements $C_i(k)$ for carts 1 to 3. It can be seen that the linearity varies among the carts. The largest deviations are obtained for cart 2 (between 25 and 140 μm). In order to make an accurate model for these variations, measurements with a higher resolution along the guideway are necessary. The carts were mounted on roller blocks and driven by a rack- and pinion system. According to the manufacturer variations in cart position are expected with a period corresponding to the length between the rack teeth, which is much shorter than the resolution of the measurements.

In Fig. 6, the residuals are decomposed into a part parallel to the track direction (projected on the linear track model) and a part orthogonal to it (the distance of the measured point to the modeled track) and shown with the respective values for measurement set 3. The angle, i.e. where on a circle around the track with a given distance the measured point was, is not shown here. The laser tracker position was different for measurement sets 2 and 3 and the exact coordinate transformation between the two can be determined except for this angle.

It can be seen that cart 2, and to a smaller extent cart 3, has a shifting error along the track direction. With only 28 measurement points along the track it is not possible to identify a spatial high frequency variation of the residuals along the tracks. It was impossible to perform further measurements within the scope of this article since the robot was dismantled after the measurements. While cart 1 is most linear and least sensitive to the small load changes induced by different TCP positions in a plane orthogonal to the track, a linear model of cart 2 will improve the TCP positioning accuracy considerably. The difference between measurements 2 (black line) and 3 (grey stars) is larger for the orthogonal errors.

D. Kinematic Error Model

In this section, kinematic error models for the linear actuators and the arm structure are presented.

For the linear actuators, the T-Mac measurements on the guideways described above are used for a piecewise linear model instead of the nominal model (2). As the 28 measure-

ments per cart did not cover the complete track, the model is only valid within the measured range [-650,700] mm.

The cart position C_i for the commanded actuator position q_i is now interpolated linearly between the two cart measurements ${}^m C_i^k$ and ${}^m C_i^{k+1}$ whose corresponding actuator positions q_i^k and q_i^{k+1} are closest to q_i :

$$C_i(q_i) = {}^m C_i^k + \frac{q_i - q_i^k}{q_i^{k+1} - q_i^k} \left({}^m C_i^{k+1} - {}^m C_i^k \right) \quad (4)$$

C_i in Eq. 4 is, unlike C_i in Eq. 2, expressed in the coordinate system used for measurement set 2. Instead of optimizing the track direction v_i and offset ${}^s C_i^0$ as for the nominal model, the coordinate frame transformation between track and TCP measurement frame has to be calibrated.

For the kinematic error model of the arm structure, all 6 links have been taken into account (see Fig. 2) as well as the TCP orientation errors that arise if the links in one cluster have slightly different lengths or if the joint placement on carts and end-effector is not according to the Tau configuration.

The closure equation for link i is then:

$$L_i^2 - \|T + R_T \cdot P_i - C_i\|_2^2 = 0. \quad (5)$$

IV. RESULTS

A. Calibration Results

To evaluate the kinematic modeling in the previous section, the calibration results of different combinations of actuator and arm structure models are compared.

Fig. 7 illustrates the different models: Model 1 is the nominal kinematics with linear actuators and a reduced arm structure. Model 2 includes the piecewise linear actuator models, combined with the reduced arm structure. Model 3 assumes linear actuators and a full arm structure model, where one distinct linear path is considered for each of the spherical joints connected to the 6 links. Model 4 combines the full arm structure model with the piecewise linear actuator model, even here with one distinct path per link. To obtain the highest possible accuracy, a fifth model was introduced which uses for each link the optimal model: Link 1 was modeled using model 3's link 1, for both cart 2 links the respective links of model 4 were used and for the 3 cart 3 links the respective links of model 3.

The cost function for the kinematic calibration was for all models the squared sum of the residuals of the closure equation (1) and (5) respectively with (2) or (4) for the actuator model. Each link was optimized individually, so the cost function for link 1 and the simple model was e.g.:

$$f_1 = \sum_{j=1}^N (L_1^2 - \|T_j - {}^s C_{1,j}\|_2^2)^2 \quad (6)$$

The measurements available for the calibration and validation consist of the 176 TCP measurements described in Sect. III-C. Removing the robot poses whose cart positions exceed the range of the piecewise linear actuator models and reserving half of the measurements for validation, 61 measurement poses are used to calibrate the four models.

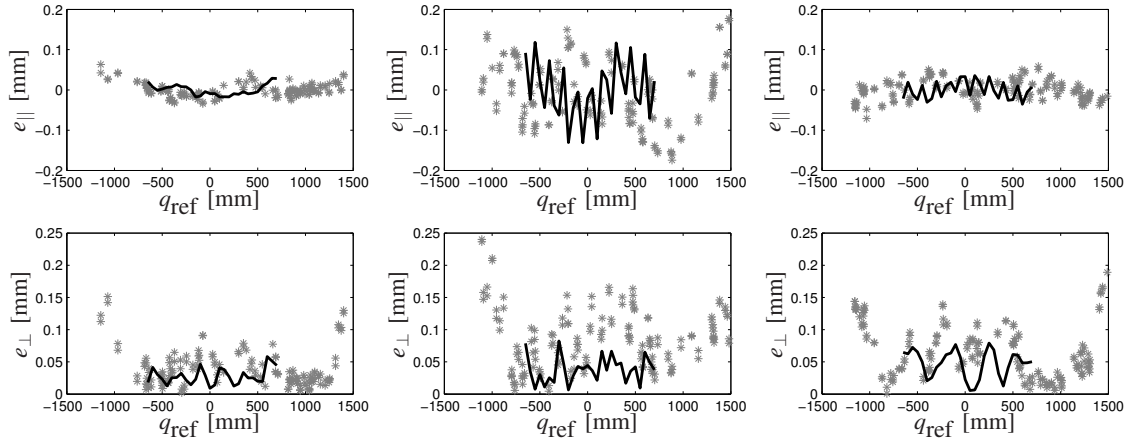


Fig. 6. Linearity errors of actuators: Residuals when fitting a linear function to the movement of cart 1 (left), cart 2 (center) and cart 3 (right). The upper row shows the residual vectors projected on the track direction, the lower row the absolute value of the residual component orthogonal to the track direction. The solid lines correspond to a TCP movement parallel to the track directions, while the grey stars represent measurements taken while the TCP was moving randomly through the workspace.

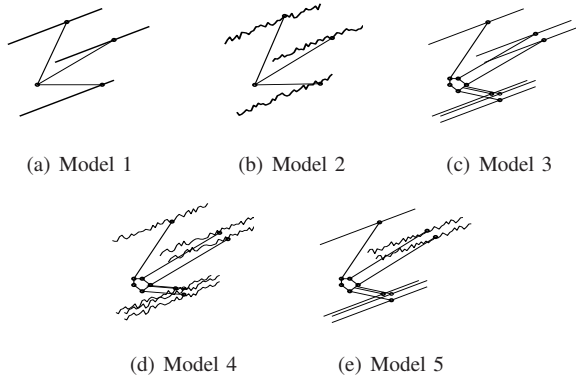


Fig. 7. Illustration of the kinematic models compared

TABLE I
ABSOLUTE POSITIONING ERROR

Model	Mean [μm]	Max [μm]
1	140	410
2	120	440
3	110	260
4	100	340
5	90	240

Table II shows the calibration results: the optimized parameters and final cost function values for each model and link. For models 1 and 3, the offsets and direction of the tracks are given, while for models 2 and 4, the coordinate frame transformations between the track measurements from set 2 and the TCP measurements from set 1 are given.

Table I shows the absolute TCP positioning error of models 1 to 5. The mean positioning error was decreased from 140 (model 1) to 90 μm (model 5) and the highest peak decreased from 410 μm (model 1) / 440 μm (model 2) to 240 μm (model 5).

Fig. 8 shows the modeling errors of the end-effector orientation changes for models 3 to 5. All models capture

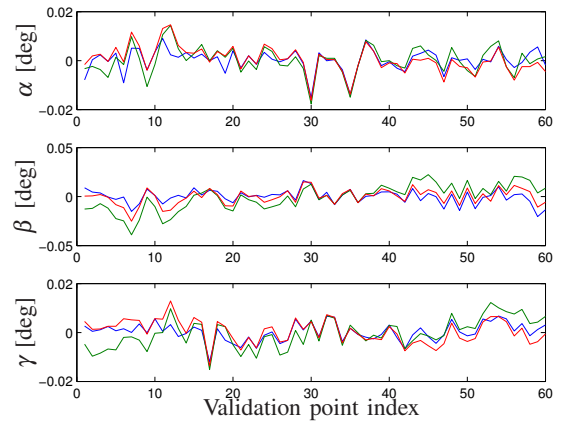


Fig. 8. Modeling error of platform orientation given in ZYZ Euler angles (see Fig. 4) for model 3 (blue), model 4 (green) and model 5 (red).

the varying orientation with only small errors. This is in accordance with the assumptions that the orientation errors are caused by kinematic errors in the arm system and not because of variations of the orientation of the carriages.

B. Parameter Sensitivity Analysis

The sensitivity of the TCP positioning and orientation error on the kinematic parameters was examined. Based on the optimized parameters, each of the 60 parameters was changed with $\pm 5 \cdot 10^{-5}$. For each parameter and link, the changes in TCP positioning ($S_{j,\text{pos}}$), TCP orientation ($S_{j,\text{rot}}$) and of the cost function ($S_{j,\text{cost}}$) are summed up for all validation points :

$$S_{j,\text{pos}} = \sum_{j=1}^N (\|T_j - T_j^+\|_2 + \|T_j - T_j^-\|_2), \quad (7)$$

where T_j is the modeled TCP position for the validation point j and T_j^+ and T_j^- the calculated TCP positions for the changed models.

TABLE II
CALIBRATION RESULTS

Model	Link	L_i [m]	P_i [m]	Track offset ${}^s C_i^0$ [m]	Track orientation Track direction v_i	Final Cost
1	1	2.04423		(-3.12999, -4.88145, 0.70473)	(0.99779, -0.06634, -0.00530)	5.458e-06
	2	2.04292		(-3.07865, -3.47376, 0.66795)	(0.99752, -0.06598, -0.00544)	3.661e-06
	3	2.04350		(-3.13955, -4.81373, -0.68032)	(0.99769, -0.06603, -0.00509)	3.515e-07
2	1	2.04423		(1.81040, -4.29494, -0.08075)	(137.94642, -0.49443, 0.36210)	5.506e-06
	2	2.04291		(1.41419, -3.86450, 0.08531)	(149.73731, -0.85832, 0.30077)	2.4647e-06
	3	2.04350		(0.53097, -2.08460, 0.03851)	(167.03480, -0.41249, 0.06433)	5.5341e-07
3	1	2.04422	(-0.04871, -0.05363, -0.10361)	(-3.18514, -4.96829, 0.77830)	(0.99773, -0.06636, -0.00544)	2.5339e-06
	2a	2.04291	(-0.05079, -0.11527, -0.08175)	(-3.13100, -3.52723, 0.79856)	(0.99761, -0.06584, -0.00544)	2.9384e-06
	2b	2.04294	(-0.05864, 0.00230, 0.13871)	(-3.12578, -3.33374, 0.64030)	(0.99744, -0.06589, -0.00562)	2.8946e-06
	3a	2.04351	(-0.18926, -0.09046, 0.04200)	(-3.32073, -4.73900, -0.59428)	(0.99766, -0.06600, -0.00515)	4.4596e-07
	3b	2.04352	(-0.04625, -0.00142, -0.14303)	(-3.19764, -4.94939, -0.65117)	(0.99764, -0.06607, -0.00507)	3.108e-07
	3c	2.04352	(-0.05438, 0.11726, 0.07666)	(-3.19209, -4.75506, -0.80852)	(0.99774, -0.06597, -0.00507)	5.6626e-07
4	1	2.04422	(-0.04871, -0.05363, -0.10361)	(1.75525, -4.38178, -0.00718)	(137.94642, -0.49443, 0.36210)	2.6253e-06
	2a	2.04291	(-0.05079, -0.11524, -0.08174)	(1.36183, -3.91799, 0.21592)	(149.73731, -0.85832, 0.30077)	1.6629e-06
	2b	2.04294	(-0.05865, 0.00234, 0.13867)	(1.36706, -3.72450, 0.05766)	(149.73731, -0.85832, 0.30077)	1.5159e-06
	3a	2.04351	(-0.18926, -0.09045, 0.04202)	(0.34979, -2.00983, 0.12452)	(167.03480, -0.41249, 0.06433)	1.1687e-06
	3b	2.04353	(-0.04625, -0.00144, -0.14303)	(0.47288, -2.22024, 0.06763)	(167.03480, -0.41249, 0.06433)	1.3091e-06
	3c	2.04353	(-0.05434, 0.11733, 0.07667)	(0.47844, -2.02590, -0.08971)	(167.03480, -0.41249, 0.06433)	4.3551e-07

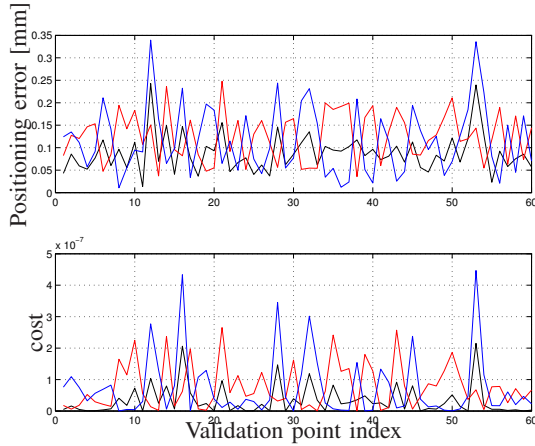


Fig. 9. Changed cost (lower) and absolute positioning error (upper) for increasing (red) and decreasing (blue) L_1 with $50 \mu\text{m}$. The original cost is shown in black; the maximum positioning error peak can be found in the cost function for arm 1, but not in the other arms' cost functions.

Similarly, the orientation changes (expressed in Euler angles) are accumulated in $S_{j,\text{rot}}$ and the cost function contribution of each measurement point in $S_{j,\text{cost}}$.

With the given measurement data and using model 5, the results shown in Table III and 10 were obtained. Within the given range of $[-650, 700]$ mm for the actuators, the modified track directions v_i result in the smallest TCP positioning changes, while the rotation matrix of the transformation between the 2 different laser tracker positions gives larger variations, as the distance from the initial cart position magnifies the $5 \cdot 10^{-5}$ change. For both the joint offsets on carts and end-effector plate the cost function is much more sensitive to the x component than to the y and z components (coordinate system see in Fig. 2). The link lengths L_i (see Fig. 9 for L_1) result in the largest sensitivity.

V. DISCUSSION

Considering Fig. 5, it appears reasonable that cart 1 gains the least by a piecewise linear instead of a linear actuator

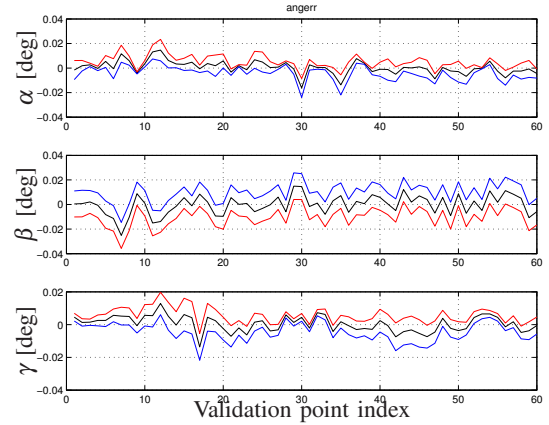


Fig. 10. Changed orientation errors for increasing (red) and decreasing (blue) $P_{x,3}$ about $50 \mu\text{m}$.

modeling, while improved results can be expected for cart 3. Cart 2 is least linear with a large error along the track direction, but the measured position for one commanded cart position varied as well significantly if the arm structure was in a different configuration, i.e. the other two carts were in different positions. This may be due to lacking stiffness which causes the cart to move with changing load of the arm structure and makes it difficult to model the actuator as presented. Since stiffness parameters were not modeled, this error source could not be compensated for.

A comparison with Table II shows as expected that a piecewise linear modeling of cart 1 does not decrease the cost function, but on the contrary increases it somewhat. The results for cart 2 in Fig. 5 indicate that a piecewise linear actuator model would not catch the cart position's dependency on the TCP's $Y-Z$ position. Nevertheless, the cost function could be decreased by using a piecewise linear actuator model. In model 4, link 2b has a slightly lower cost function than link 2a. This can be explained by the fact that the T-Mac was mounted closer to the link 3 joint during the

TABLE III
PARAMETER SENSITIVITY

Link	1	2a	2b	3a	3b	3c
TCP positioning change $S_{j, \text{pos}}$						
L_i	11.6	5.9	3.8	2.0	5.6	2.9
$P_{i,x}$	9.1	5.1	3.4	1.6	4.6	2.4
$P_{i,y}$	3.2	2.3	1.4	0.8	2.3	1.2
$P_{i,z}$	5.7	1.2	0.8	0.7	1.9	1.0
Offset _x	9.5	4.9	3.2	1.7	4.8	2.5
Offset _y	4.2	2.0	1.3	0.6	1.9	0.9
Offset _z	4.4	2.1	1.4	0.6	1.7	0.9
Orient.	2.7	7.0	4.5	0.5	1.3	0.7
Orient.	1.3	5.9	3.7	0.2	0.5	0.2
Orient.	1.3	3.6	2.2	0.2	0.5	0.3
Angular error change $S_{j, \text{rot}}$						
L_i	3.7e-05	0.048	0.048	0.038	0.049	0.05
$P_{i,x}$	2.9e-05	0.042	0.042	0.031	0.04	0.042
$P_{i,y}$	1.2e-05	0.018	0.018	0.015	0.019	0.019
$P_{i,z}$	1.8e-05	0.0094	0.0094	0.013	0.017	0.017
Offset _x	3e-05	0.04	0.04	0.033	0.042	0.044
Offset _y	1.3e-05	0.015	0.015	0.012	0.017	0.016
Offset _z	1.6e-05	0.017	0.017	0.011	0.014	0.014
Orient.	8.5e-06	0.053	0.053	0.009	0.012	0.012
Orient.	3.9e-06	0.046	0.046	0.0032	0.0043	0.0042
Orient.	4.8e-06	0.028	0.027	0.003	0.0039	0.0039
Cost function change $S_{j, \text{cost}}$						
L_i	8.2e-06	7.4e-06	8.2e-06	5.8e-06	5.3e-06	5.8e-06
$P_{i,x}$	6e-06	6.2e-06	7e-06	4.3e-06	3.9e-06	4.4e-06
$P_{i,y}$	2.1e-06	2.3e-06	2.7e-06	1.8e-06	1.4e-06	1.9e-06
$P_{i,z}$	3.9e-06	1.2e-06	1.5e-06	1.4e-06	1.2e-06	1.6e-06
Offset _x	6.2e-06	5.9e-06	6.6e-06	4.6e-06	4.2e-06	4.7e-06
Offset _y	2.8e-06	2e-06	2.4e-06	1.3e-06	1.1e-06	1.5e-06
Offset _z	3e-06	2.2e-06	2.6e-06	1.4e-06	1e-06	1.4e-06
Orient.	1.5e-06	1e-05	1.1e-05	9.7e-07	7.8e-07	1e-06
Orient.	8.6e-07	8.7e-06	9e-06	3.2e-07	2.5e-07	3.6e-07
Orient.	8.8e-07	4e-06	4.5e-06	3.5e-07	2.4e-07	3.5e-07

measurements, which model thus the link 3 joint movement better than that of the link 2 joint on the same cart. The cost function of cart 3 on the other hand decreases when including a piecewise linear actuator model. While the cost function for link 3c in cart 3, which was the one nearest to the T-Mac during measurements, could be reduced somewhat from model 3 (linear actuators) to model 4, the cost functions for links 3a and 3b increased to 2.6 and 4.2 times, respectively, their values for model 3.

Even though the resulting accuracy was not as low as expected in relation to the repeatability level, these results show the potential of an improved actuator modeling, where attention to the exact position of all spherical joints on a cart, the dependency on the movement and position of the other carts and stiffness should be paid.

A comparison of the carts shows that the cost of cart 3 is in general about a factor 10 lower than that of carts 1 and 2, among which cart 1 tends to perform worse than cart 2. An explanation for this may be, together with the actuator performance from Fig. 5, that in general, the more links an arm consists of, the stiffer it is.

The kinematic error model of the arm structure gave better results than the nominal model in all cases except for cart 3.

The models including all 6 links (models 3 to 5) manage to capture the varying TCP orientation. Overall, the angular modeling is better and gives lower errors than the positioning. Another interesting point is that the angular errors of the nominal kinematics (Fig. 4) exhibit a repeating pattern, which may be caused by errors in the arm structure modeling,

unlike the positioning errors do, which may indicate that the remaining positioning errors can be decreased further by a better actuator modeling. The peak positioning error increases for the models with a piecewise linear actuator modeling. That may indicate that the corresponding pose, which is at the edge of the robot workspace, is particularly sensitive to the actuator modeling.

The parameter sensitivity analysis shows that more attention needs to be paid to the excitation of the different parameters by the chosen measurement points. In particular, the TCP measurement points should cover a larger range in x-direction to give a better excitation for the track directions c_j .

VI. CONCLUSION AND FUTURE WORK

In this article, a new kinematic error model for a parallel kinematic Gantry-Tau robot was presented. The kinematic error model included a piecewise linear model of the prismatic actuators and a full model of the robot's arm structure. The modeling assumptions of the nominal kinematics were examined using laser tracker measurements. Four different combinations of nominal kinematics and error kinematic model parts were evaluated by their calibration results.

The modeling purpose was to evaluate the maximum possible positioning accuracy which varied from 140 μm to 90 μm between the different models. With stiffness modeling and additional measurements on the actuators with higher positional resolution, the positioning error can be reduced even further in the future to fully benefit from the Gantry-Tau's high accuracy.

For accurate movements at high speed, dynamic modeling of the Gantry-Tau will be developed further.

REFERENCES

- [1] J.-P. Merlet, *Parallel Robots*, Kluwer Academic Publishers, Norwell, MA, 2000.
- [2] L. Johannesson, V. Berbyuk and T. Brogårdh, "Gantry-Tau – A New Three Degrees of Freedom Parallel Kinematic Robot", in *Proc. 4th Chemnitz Parallel Kinematics Seminar*, 2004, pp. 731-734.
- [3] T. Brogårdh, *A device for relative movement of two elements*, Patent WO 97/33726, 1996.
- [4] H. Cui, Z. Zhu, Z. Gan and T. Brogårdh, "Kinematic analysis and error modeling of TAU parallel robot", in *Robotics and Computer-Integrated Manufacturing*, Vol.21, 2005, pp.497-505.
- [5] I. Williams, G. Hovland and T. Brogårdh, "Kinematic Error Calibration of the Gantry-Tau Parallel Manipulator", in *Proc. Int. Conf. on Robotics and Automation*, Orlando, FL, 2006, pp.4199-4204.
- [6] I. Dressler, A. Robertsson and R. Johansson, "Accuracy of Kinematic and Dynamic Models of a Gantry-Tau Parallel Kinematic Robot", in *Proc. Int. Conf. on Robotics and Automation (ICRA'07)*, Rome, 2007.
- [7] P. Crothers, K. Siercks, P. Freeman, T. Brogårdh, I. Dressler, K. Nilsson, A. Robertsson, W. Zulauf, B. Felber and R. Loser, "Characterisation of the ABB Tau Parallel Kinematic Machine for Aerospace Application", in *SAE 2009 AeroTech Congress*, Seattle, WA, 2009.
- [8] J. Wang and O. Masory, "On the accuracy of a Stewart platform. I. The effect of manufacturing tolerances", in *Proc. Int. Conf. on Robotics and Automation (ICRA'93)*, Atlanta, Georgia, 1993.
- [9] Leica Geosystems, homepage:
<http://www.leica-geosystems.com> (2009).
- [10] SMErobot™ homepage:
<http://www.smerobot.org> (2009).